Central European Journal of Energetic Materials
ISSN 1733-7178; e-ISSN 2353-1843

Cent. Eur. J. Energ. Mater. 2017, *14*(3): 636-659; DOI: 10.22211/cejem/75980

Thermal Decomposition Characteristics of Ammonium Nitrate(V) in the Presence of Mn_2O_3/Graphene Oxides

Zhixiang Xu,* Guisheng Xu, Xiaoqi Fu, Qian Wang

School of Energy and Power Engineering, Jiangsu University, Xuefu road 301, Zhenjiang, Jiangsu Province, 212013 Zhenjiang, China
**E-mail: xuzx@ujs.edu.cn*

Abstract Nano-composites (Mn_2O_3, Mn_2O_3/graphene oxides (GO)) were prepared by a new method. The nano-composites were characterized by XRD and HRTEM. The catalytic performance of the nano-composites on the thermal decomposition of ammonium nitrate(V) (AN) was investigated by TG-DSC and TG-MS. The reaction of AN with the nano-composites in the condensed phase was investigated by RSFTIR. The results of TG-DSC experiments indicated that the nano-composites significantly catalyze the thermal decomposition of AN, especial Mn_2O_3/GO. The exothermic reaction of AN with Mn_2O_3/GO commenced at about 185 °C. Based on the TG-MS results, it was ascribed to N_2O formation. In the RSFTIR experiments, the dissociation reaction and ionization reaction of AN were both detected. NOx formation at low temperature was also found. NH_2 was directly oxidized by HNO_3/NO_3^- at low temperature. The interaction between Mn_2O_3 and NH_3 was detected according to DRIFT experiments. At elevated temperature, the functional groups of GO are destroyed, which had an influence on the interaction between Mn_2O_3 and GO. A probable mechanism for the exothermic reaction and then its disappearance is proposed. HNO_3 gas was absorbed on the surface of solid AN, which can markedly catalyze the thermal decomposition of AN. Perhaps the HNO_3 plays a key role in the exothermic reaction and then the reaction of AN disappears at very low temperatures.

Keywords: ammonium nitrate(V), nano-oxide, graphene oxides, thermal decomposition, RSFTIR

1 Introduction

Ammonium nitrate(V) (AN) is widely applied as a fertilizer and is a component in a variety of energetic compositions, especial in industrial explosives. AN is also used as an oxidizer in propellant formulations for the reduction in the use of

ammonium perchorate. The products from AN are environmentally friendly, and AN's smokeless combustion has caused AN-based composite propellants to receive much attention. Furthermore, AN propellant formulations are relatively insensitive over a wide range of temperatures, *i.e*. mechanical sensitivity and heat sensitivity. An important drawback of AN is its endothermic reaction in the initial stages of AN decomposition. This distinctive property of AN has caused poor ignitability, low energy and a low burning rate. Another important property is the transitions between several crystalline phases of AN, especially at room temperature. Hence, these poor properties limit the application of AN in solid rocket propellants [1-4]. Several additives, such as cupric oxide and potassium nitrate(V), have been reported to stabilize AN against phase change, and to reduce hygroscopicity. A further advantage is an increase in the burning rate of AN. It is known that transition metals are effective additives for decreasing the thermal decomposition temperature of AN and for increasing the burning rate of AN based propellants [5-13].

Graphene is a special type of carbon material. It has attracted great attention in recent years for its unique electrical, catalytic and mechanical properties [14, 15]. A typical property of graphene is its huge surface area, which is very important for catalytic reactions. Therefore, it has attracted much attention in catalysis. Many researchers have reported graphene or graphene oxide (GO) use in propellants as an additive [16-21]. However, less literature has reported graphene or GO as a supporter to catalyze AN. Therefore, we were very interested in developing GO composites with nano-materials to catalyze AN.

For its excellent low temperature catalytic performance, Mn_2O_3 has attracted much interest in NH_3-SCR [22-24]. Mn_2O_3 has also been reported to catalyze AN thermal decomposition [5, 6]. However, there is little literature on the mechanism of thermal decomposition. On the other hand, as is well known, pure nano-particles are easily aggregated, which would cause the catalyst efficiency to be decreased. Therefore, GO may be an ideal catalyst supporter to inhibit aggregation of nano-particles. Based on this analysis, we hoped that GO could dramatically inhibit aggregation of nano-particles in the AN thermal decomposition process, thus improving the catalytic activity.

In this paper we report a new method for the preparation of Mn_2O_3 nano-composites. The catalytic effect of Mn_2O_3 and Mn_2O_3/GO nano-composites on the thermal decomposition of AN was investigated by TG-DSC and compared with that of pure AN. The evolved gases were analyzed to investigate the thermal decomposition mechanism. In order to analyze the interactions between Mn_2O_3, AN and GO, we also carried out RSFTIR (Remote Sensing Fourier Transform Infrared: RS-FTIR) experiments. The interaction between Mn_2O_3 and NH_3 was also studied by DRIFT (Diffuse Reflectance Infrared Transform spectroscopy:

DRIFT) experiments. The activation energy of the samples was calculated using the Ozawa method. A catalytic mechanism of AN with Mn_2O_3/GO is proposed.

2 Experimental

2.1 Materials

$Mn(NO_3)_2$ aqueous solution (50%) (AR), and NH_4NO_3 (AR) were used without further purification. Sorbitan mono-oleate (SMO) and diesel oil were industrial materials. GO was made in house from purified natural graphite (230 mesh, Qingdao Zhongtian Company) according to the method reported by Hummers and Offeman [25].

2.2 Synthesis and characterization of the nano-catalyst

2.2.1 Synthesis of Mn_2O_3 nano-catalyst by a new method

Nano Mn_2O_3 was synthesized by a new method. This method afforded nano-particles more readily than the auto-combustion method. The method did not need a dehydration stage. A low calcination temperature, accurate measurement and auto-combustion properties made this method easier for the synthesis of the nano-oxide. The procedure for generating nano-particles has two steps: (1) preparation of an emulsion; (2) calcination of the emulsion in a furnace. The formation of the emulsion was as follows:

water : AN : $Mn(NO_3)_2$ solution : SMO : diesel oil = 16 : 38 : 40 : 1.5 : 4.5

(1) Preparation of the emulsion

Two steps were involved in the emulsion preparation. Firstly, the oxidizer solution and the oil phase were prepared. The ingredients of the oxidizer solution, which included water, AN and $Mn(NO_3)_2$ solution, were mixed in a large stainless steel beaker. After dissolution, the oxidizer solution was maintained at a temperature of approximately 80 °C. The oil phase, which included SMO and diesel oil, was poured into the mixer bowl and the temperature was maintained at 60 °C. After the oxidizer solution and oil phase had been prepared, mixing was commenced at a speed of ca 200 rpm. In the second step, the hot oxidizer solution was poured slowly into the bowl. After the addition, the speed of mixing was accelerated (to ca 1200 rpm) and continued for a few seconds to achieve the final refinement.

(2) Calcination of the emulsion in a furnace

The emulsion sample was then calcined in a furnace at 600 °C. After 2 h heating,

the solid Mn_2O_3 nano-particles were collected. The solid was washed with ethanol and then used for further experiments. The nano-particles were characterized by XRD and HRTEM.

2.2.2 Synthesis of the Mn_2O_3/GO nano-catalyst and sample preparation

The Mn_2O_3/GO nano-composite was synthesized in the following procedure. GO powder (100 mg) and n-butylamine (5 mL) were dispersed in water (100 mL) by sonication, forming a stable graphene oxide colloid. After 1 h, a dispersion of Mn_2O_3 (200 mg) sonicated in water (100 mL) and ethylenediamine (5 mL) was added to the graphene oxide colloid solution. Subsequently, the mixture was heated at 60 °C with magnetic stirring for 6 h. Bulk samples can be obtained by centrifugation of the mixture, and then washed several times with deionized water and ethanol. The Mn_2O_3/GO nano-composite was obtained after the precipitate had been dried at 60 °C under vacuum for 12 h.

For the studies on the catalytic activity of AN thermal decomposition, Mn_2O_3 and Mn_2O_3/GO nano-catalyst were each mixed separately with AN in the weight ratio 98:2 wt.% by blending with a mechanical stirrer. The samples were named as follow:

1# 2% Mn_2O_3 + AN;

2# 2% Mn_2O_3/GO + AN.

2.3 XRD and HRTEM analysis

The powder X-ray diffraction (XRD) analyses of the samples were carried out with a Bruker D8 Super Speed apparatus operating with Cu Kα radiation. High-resolution transmission electron microscopy (HRTEM) was carried out by means of a field emission electron microscope, Tecnai G2 F30 S-TWIN, operating at 300 kV.

2.4 Thermal decomposition of AN samples

Thermal decomposition experiments of the samples were carried out in a nitrogen atmosphere with a NETZSCH STA449C instrument. The sample (10 mg) was loaded into a closed ceramic crucible with a pinhole in the cap. Nitrogen, at a flow rate of 20 mL/min, was used as the purge gas. Non-isothermal curves were recorded at heating rates of 2.5 K/min, 5, K/min 10 K/min and 20 K/min. The samples were heated from room temperature to 400 °C.

2.5 RSFTIR experiments

RSFTIR measurements were conducted using a Nicolet Model NEXUS 870 FT-IR Instrument and an *in situ* thermolysis cell (Xiamen University, China)

in the temperature range 20-500 °C. Argon at a flow rate of 10 mL/min was used as the purge gas. The heating rate was selected as 10 K/min. KBr pellet samples were used, by thoroughly mixing about 1.5 mg samples and 120 mg KBr. Infrared spectra in the range 4000-500 cm^{-1} were obtained using a model DTGS detector at a rate of 15 files/min and 10 scans/file, with 5 cm^{-1} resolution.

2.6 TG-MS experiments

The TG-MS tests were performed with a TG-DSC (NETZSCH STA449C) system and MS (NETZSCHQMS403C) system. The NETZSCH-QMS403C conditions were: ionizing electron energy 70 eV, quartz capillary gas connector, pressure injection 1,000 mbar. Approximately 2 mg samples were heated from room temperature to 360 °C. The heating rate was 10 K/min, and the samples were held in Al_2O_3 crucibles. High-purity nitrogen was used as the purge gas, with a gas flow rate of 20 mL/min.

2.7 Diffuse reflectance infrared transformation spectroscopy (DRIFT) experiments

FTIR spectra were acquired using an *in situ* DRIFT cell equipped with a gas flow system. The DRIFT measurements were performed with a Nicolet IS (IZ) 10 FTIR spectrometer, at 4 cm^{-1} resolution. The range of the spectra was 650-4000 cm^{-1}. In the DRIFT cell, the catalyst was pre-treated at 573 K in an N_2 environment for 1 h, and then cooled to room temperature. The background spectrum was recorded with N_2 flowing and was subtracted from the sample spectrum. The flow rate of NH_3 was 20 mL/min. The experimental temperature range was 110-200 °C.

2.8 Decomposition kinetics analysis

There are many methods available for calculating kinetic data. The Kissinger method has been applied widely to determine kinetic data due to its ease of use. However, accurate E values require $G(\alpha)$ to be independent of the heating rate. Another important fault is that this method produces only a single activation energy value. However the actual reaction process is very complex. Hence, the activation energy in this paper was calculated by iso-conversional methods that utilize TG data at different heating rates. The heating rates were 2.5 K/min, 5 K/min, 10 K/min and 20 K/min. The activation energy of the AN thermal decomposition, with and without nano-particles, can be determined using the Ozawa method [26]. The model used a correlation of the heating rate of the samples, activation energy and inverse temperature. The equation was as follows:

$$\lg\beta = \lg\left(\frac{AE}{RG(\alpha)}\right) - 2.315 - 0.4567\,\frac{E}{RT} \quad (1)$$

where β is the heating rate (K/min), A is pre-exponential factor, E is the activation energy, R is the universal gas constant, and $G(\alpha)$ is the mechanism function. The slope of the linear plot of lg β against the inverse temperature was used to obtain the activation energy for each conversion step.

3 Results and Discussion

3.1 Characteristics of the nano-catalysts

The nano-composites were initially characterized by XRD and HRTEM. Figure 1 shows the XRD patterns of the as-synthesized Mn_2O_3 and Mn_2O_3/GO composites. The diffraction peaks were located in the range of 20° to 80° and were all ascribed to the characteristic Bragg reflections of Mn_2O_3 (JCPDS 78-0390). No obvious diffraction peaks of GO were observed. This indicated that the Mn_2O_3 particles were attached to the GO surface and that the regular layered structure of GO was disrupted. Figure 2 shows the HRTEM images of the as-synthesized Mn_2O_3 and Mn_2O_3/GO. The Mn_2O_3 particles showed slight aggregation, and the average size of Mn_2O_3 was about 20 nm. The GO prevented nano-Mn_2O_3 aggregation, and most of the Mn_2O_3 nano particles were distributed randomly on the GO sheets.

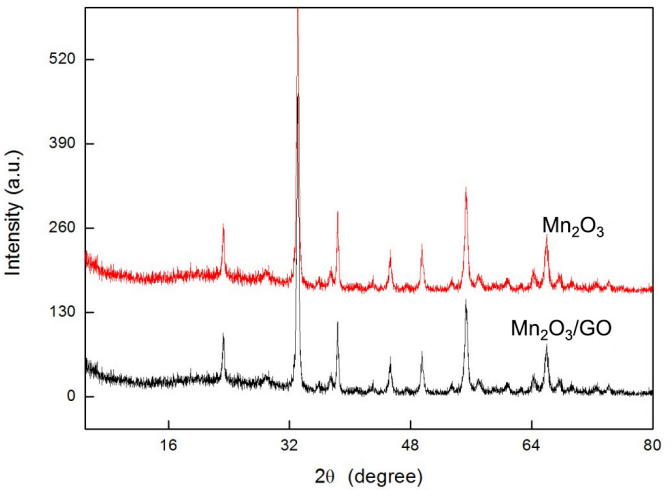

Figure 1. XRD of as-synthesized Mn_2O_3 and Mn_2O_3/GO composites

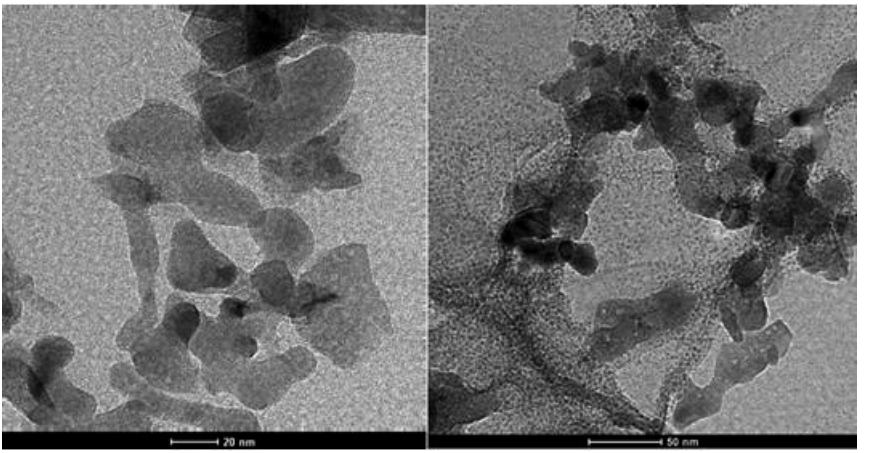

Figure 2. HRTEM images of (left) Mn_2O_3, (right) Mn_2O_3/GO composites

3.2 The influence on the thermal decomposition of AN with catalysts

The performances of Mn_2O_3 and Mn_2O_3/GO composite on the thermal decomposition of AN were investigated by TG-DSC. The results are presented in Figure 3. The Refs. [17, 18] have found that GO has little influence on the thermal decomposition of ammonium perchorate, even at a high temperature (400 °C). Hence GO itself was not reinvestigated for catalyzing the thermal decomposition of AN, for a decomposition temperature of about 300 °C. The TG curves of Figure 3 show that Mn_2O_3/GO catalyzed significantly AN thermal decomposition. At a very low temperature (about 190 °C) there was a notable mass loss, which means the reaction was violent. Mn_2O_3 also can catalyze AN thermal decomposition, but not markedly. The DSC curves of Figure 3 revealed that the samples reacted in two stages. Prior to 170 °C, an endothermic peak appeared for the phase transition of AN. Above 170 °C, an endothermic peak indicates thermal decomposition of AN. Surprisingly, a marked exothermic reaction of 2# was observed first. The exothermic peak appeared at about 190 °C. It is very interesting that the exothermic reaction was observed first and that the reaction was at a very low temperature. No paper has reported an exothermic phenomenon for AN thermal decomposition with a catalyst at about 190 °C. In this temperature region, it is well known that the endothermic reaction of AN dominates [1, 2]. The exothermic phenomenon means that at this temperature the reaction path is changed when Mn_2O_3/GO is added to AN. At the same time, as can be seen from Figure 3, it was found that the decomposition temperature of AN with additives is shifted to a markedly lower temperature. In order to analyze how the additives influence the AN thermal decomposition, the

decomposition temperatures of the samples at different mass losses are listed in Figure 4. The results showed that the decomposition temperature of AN with additives was lower than pure AN at same mass loss, especially for AN with Mn_2O_3/GO. These results mean that Mn_2O_3/GO is an excellent catalytic agent for AN thermal decomposition. Mn_2O_3 too can catalyze AN thermal decomposition, but the catalysis was not notable. It also means that GO prevented aggregation of nano-Mn_2O_3.

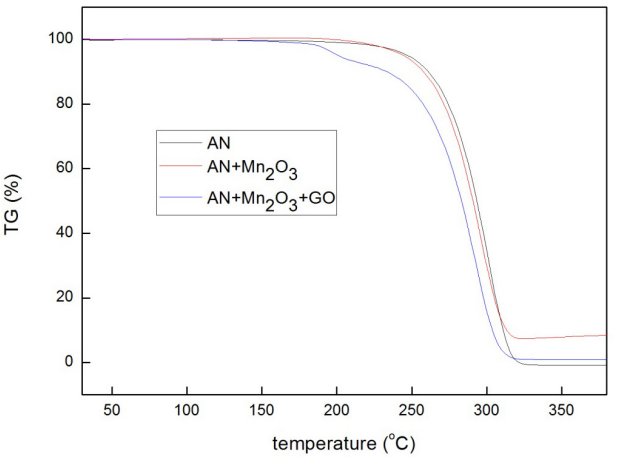

(**a**) TG curves of samples

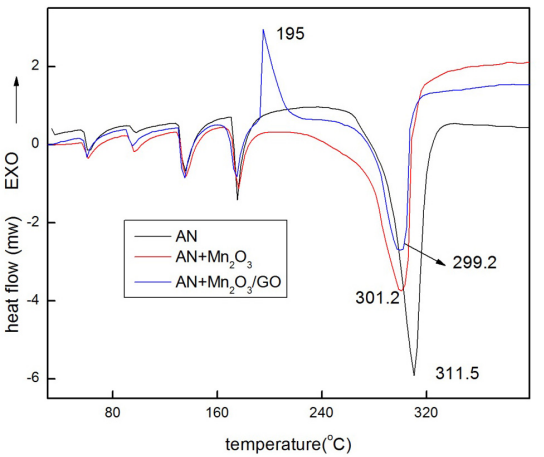

(**b**) DSC curves of samples

Figure 3. TG-DSC curves of samples at heating rate 10 K/min

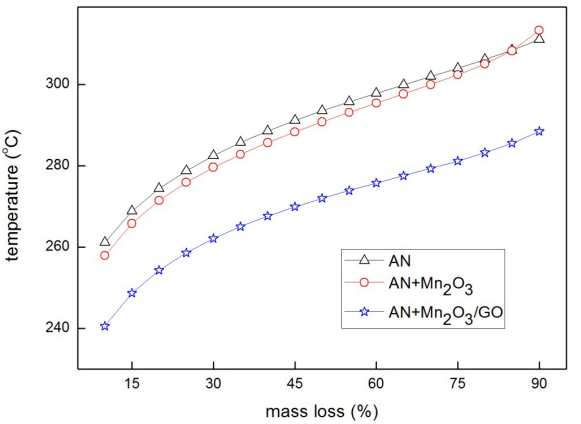

Figure 4. Decomposition temperature of samples at different mass losses

In order to analyze the catalysis by Mn_2O_3 and Mn_2O_3/GO on AN thermal decomposition, the activation energy was calculated using the Ozawa method. The results are listed in Figure 5. In the present study, the mean activation energy of pure AN was about 129 kJ/mol, which is in good agreement with the previously reported value, while the activation energy of AN with Mn_2O_3 and Mn_2O_3/GO was 119 kJ/mol and 114 kJ/mol, respectively. Hence, the activation energy of AN with additives was significantly decreased. In our previous work [27-30], we also found that active material catalyzed AN decomposition, but the differences in the absolute activation energy values were not large. From the combined Figures 3, 4 and 5, the reaction kinetics process of AN with additives was perhaps changed. Hence, we can confirm that the additives significantly catalyze AN thermal decomposition, especially Mn_2O_3/GO. However, the TG-DSC curves cannot provide adequate information about the reaction process, especially about the exothermic reaction of AN with Mn_2O_3/GO at 195 °C. Hence, TG-MS was used to analyze the thermal decomposition process of AN, with and without additives.

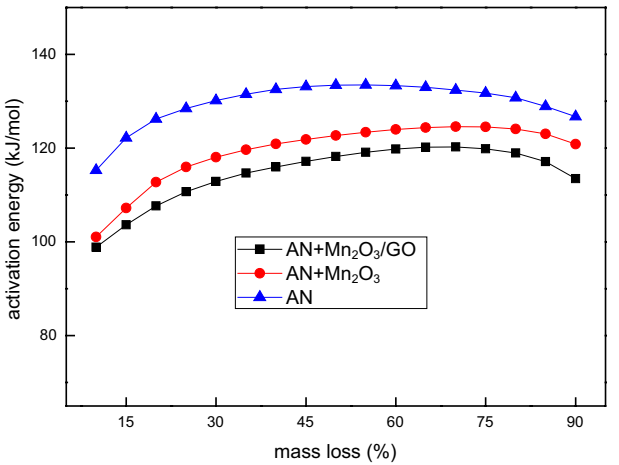

Figure 5. Activation energy of AN with and without additives

3.3 Evolved gas analysis

In order to analyze the decomposition mechanism of AN with additives in the gas phase, real-time mass spectral analysis of the evolved gases was performed. The MS analysis results are listed in Figures 6, 7 and 8. They show the ion current curves for mass-to-charge (m/z) ratios 16, 17, 18, 28, 30, 44 and 46. These peaks were assigned to NH_3 (m/z = 16, 17), H_2O (m/z = 17, 18), NO (m/z = 30), N_2 (m/z = 28), N_2O (m/z = 44) and NO_2 (m/z = 46). We have demonstrated the presence of HNO_3 in the products of AN thermal decomposition in previous work [28, 29]. It was not detected in this work.

For the dissociation reaction of AN even at low temperatures [31], the species (m/z = 17) at low temperature appeared, and was ascribed to NH_3. From Figures 6, 7 and 8, the curve changes show the presence of NH_3. The ammonia can then further decompose, but needs a higher temperature [32, 33]. In the reaction process, NO_2 (m/z = 46) was also detected. The species (m/z = 44) was perhaps N_2O. Certainly water was formed in the reaction process.

The exothermic peak for AN with Mn_2O_3/GO appeared at 195 °C in the DSC result. In Figure 8, notable changes in the ion current curves for H_2O, NH_3 and N_2O were observed at about 187 °C. However, the pure AN and AN with Mn_2O_3 systems exhibited no change at this temperature. Hence, Mn_2O_3/GO significantly catalyzed AN thermal decomposition. We can confirm that GO played an important role in this, in which it inhibited aggregation of the nano-composite.

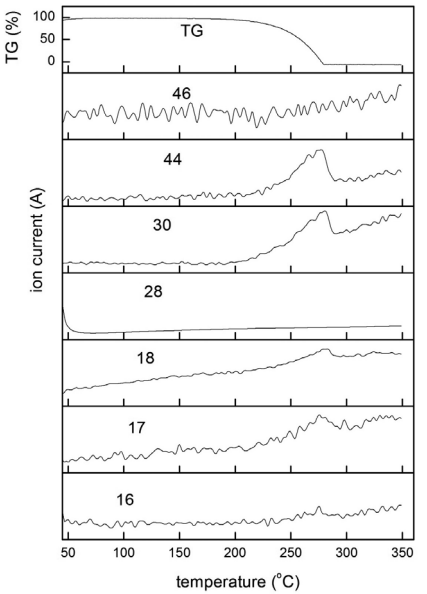

Figure 6. Mass spectra of the products of AN

From Figure 8, it may be observed that N_2O was formed at a very low temperature of about 185 °C. According to the TG-DSC and TG-MS results, it was confirmed that at about 185 °C, the exothermic reaction of AN with Mn_2O_3/GO appeared and the mass loss was accelerated. At the same time, a large amount of gas was generated. This was not observed with pure AN and AN with Mn_2O_3. In other ranges of temperature, the reaction was endothermic. In Ref. [34] it was thought that N_2O is formed when NH_3 reacts with NOx at less than 200 °C. According to the results in Ref. [35], NO_2 must be present to form N_2O. However, under the present conditions, NO_2 was very difficult to observe when the temperature was below 200 °C. The only oxidizing gas was HNO_3, and it too can be found at very low temperatures [28, 29, 36]. However, the exothermic reaction occurred at 185 °C?

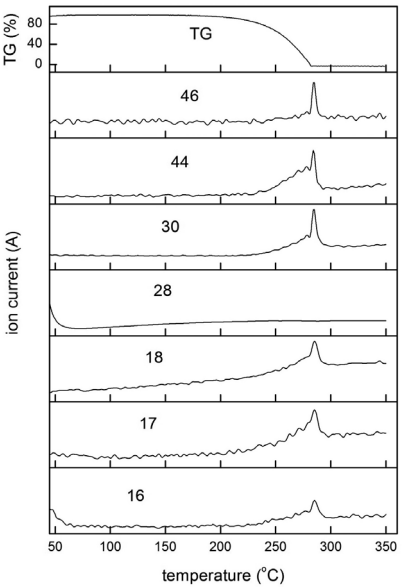

Figure 7. Mass spectra of the gaseous products of AN with Mn_2O_3

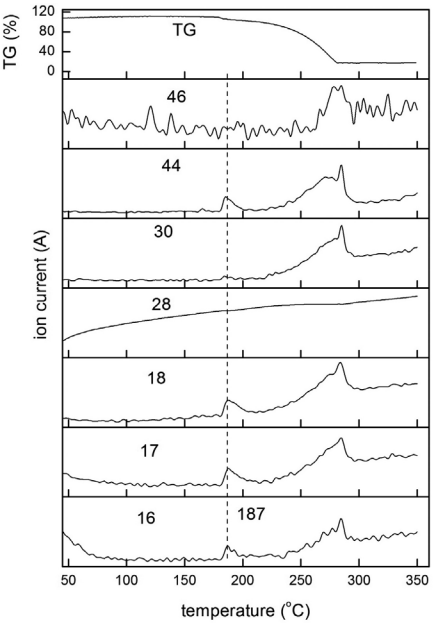

Figure 8. Mass spectra of the products of AN with Mn_2O_3/GO

3.4 RSFTIR experiments

In order to analyze the AN reaction in the condensed phase, RSFTIR experiments were carried out. The typical results for AN are shown in Figure 9. The FTIR characteristics of AN have been extensive studied [37, 38]. According to the FTIR of AN, the main characteristic peaks are for NH_4^+ and NO_3^-. The peak at 3137 cm^{-1} was assigned to the NH_4^+ asymmetric stretching vibration. The peak at 1381 cm^{-1} was assigned to the NO_3^- asymmetric stretching, and that at 1047 cm^{-1} was assigned to NO_3^- totally symmetric stretching. The peak at 826 cm^{-1} was assigned to NO_3^- out-of-plane deformation, and that at 705 cm^{-1} was assigned to NO_3^- in plane deformation. As the temperature increased, the vibration of NH_4^+ became weaker. This means that the AN dissociation reaction occurred and NH_3 was generated. However, the vibration of NH_4^+ was still present. The NO_3^- vibration was still very strong even at 250 °C with pure AN. This means that even at 250 °C, NH_4^+ and NO_3^- still appeared in pure AN. The results also support the results from reference [39]. We also found same results in our previous work [40]. However, at the elevated temperature, the primary products from AN decomposition also reacted among themselves. The peak at 1095 cm^{-1}, assigned to an N=O vibration, was perhaps ascribed to NOx [41]. Furthermore the peak at 1577 cm^{-1} was assigned to an NH_3 vibration. According to the RSFTIR experimental results for pure AN, we can see that the dissociation reaction and the ionization reaction are all present.

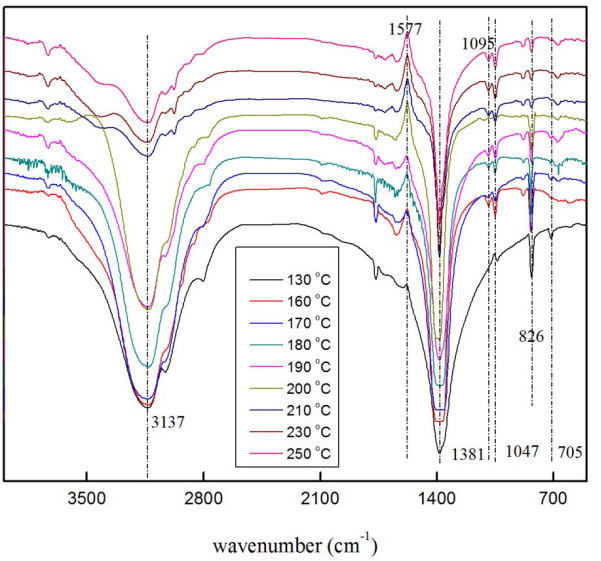

Figure 9. RSFTIR experimental results of AN

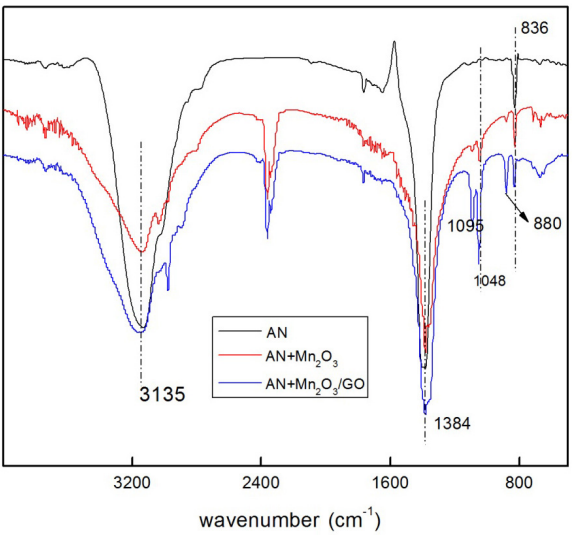

Figure 10. RSFTIR experimental results of samples at 200 °C

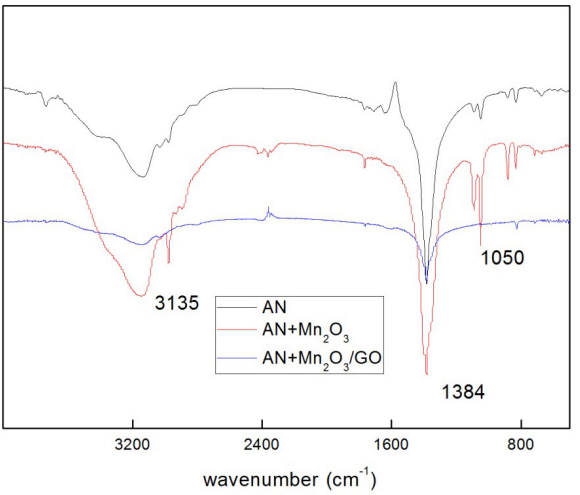

Figure 11. RSFTIR experimental results of samples at 250 °C

RSFTIR experiments of AN with additives were also carried out. In order to explore the differences between the samples, the notable results of the samples are listed in Figures 10 and 11. In Figures 10 and 11, the peak at 2360 cm^{-1} was caused by air. It was not a decomposition product of AN. According to Figure 10, the exothermic reaction of AN with Mn_2O_3/GO sample at 185 °C was

observed according to the DSC curve, but the RSFTIR experiment showed a clear difference at 200 °C. The peak at 1095 cm^{-1} was found in the 1# and 2# samples, but the 2# was violent. However, pure AN exhibited no similar reaction at this temperature. This means that Mn_2O_3 and Mn_2O_3/GO can catalyze the thermal decomposition of AN to a remarkable degree. When GO acted as a supporter to prevent Mn_2O_3 aggregation, the catalytic activity of Mn_2O_3/GO was notably increased. The same results were also found at 250 °C. In Figure 11, the NO_3^- and NH_4^+ vibrations were very weak in sample 2#, but still very strong in pure AN and sample 1#. This means that the reaction in AN with Mn_2O_3/GO was more violent than the other samples in the condensed phase. The RSFTIR results were coherent with the TG-DSC and TG-MS results. The RSFTIR experiments provided adequate information about the AN reaction in the condensed phase. These results indicated that Mn_2O_3/GO has excellent catalytic activity for AN thermal decomposition at low temperatures. We can also confirm that the NH_3 can be oxidized by HNO_3/NO_3^-. However, we cannot at present confirm that the oxidizer is HNO_3 or NO_3^- or HNO_3/NO_3^-. The reactivity of HNO_3 is stronger than NO_3^-. We still cannot explain why the exothermic reaction was disappeared.

3.5 Catalytic mechanism of the thermal decomposition of AN catalyzed by the nano-composites

Thermal decomposition of AN has been researched widely [1-3]. Many researchers have proposed a thermal decomposition mechanism. Oxley's proposed ionic and radical reaction mechanisms were widely accepted [42, 43].

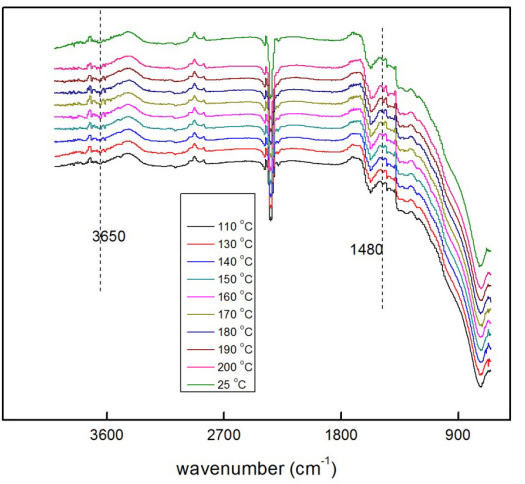

Figure 12. DRIFT experimental results

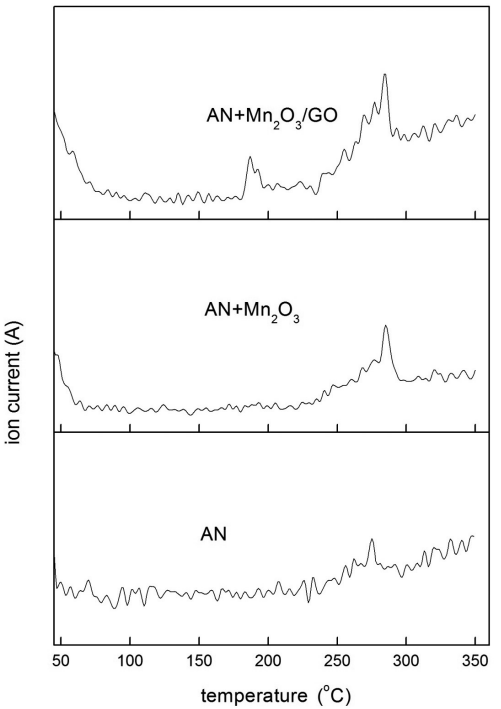

Figure 13. Ion current curve of NH_2 (m/z = 16)

GO has a large surface area, thus when ammonia and HNO_3 (g) emerge, they can be absorbed onto the nano-material surface. Certainly, the surface of particles of AN also absorb ammonia and HNO_3 (g) at low temperature. Many researchers have reported on the interaction of NH_3 and Mn_2O_3 by SCR. The interaction between NH_3 and Mn_2O_3 was studied by DRIFT. The results are listed in Figure 12. A difference was observed in the 3650 cm^{-1} and 1480 cm^{-1} absorptions, which was ascribed to NH_3 in different locations. Hence, we can confirm that the interaction happened at very low temperatures. The reaction was performed and NH_2 was formed [44-47]. If NH_2 is formed, the curve of the ion current would change. The results of the ion current curve for NH_2 are shown in Figure 13. This demonstrated that a marked difference was observed at about 185 °C. NH_2 was generated from the AN with Mn_2O_3/GO sample at about 185 °C, but then disappeared. NH_2 can be oxidized easily by oxidizing materials. We found the same tendency with the N_2O ion current curve. The N_2O was generated at about 185 °C, but later also disappeared. The ion current curve for NO_2 exhibited little change. Hence, the Ref. [35] result is wrong for

the present conditions. On the other hand, it is generally accepted that, under low temperature selective catalytic reduction reaction conditions, N_2O is formed *via* the decomposition of AN, as an intermediate formed on the catalyst when ammonia reacts with the surface nitrate groups [48-50]. Ref. [51] also proposed that three N–H bonds must be cleaved by the surface oxygen species of the manganese oxides to form N_2O. Hence, NH_2 was readily oxidized. Ref. [47] thought that both the Eley-Rideal mechanism and the Langmuir-Hinshelwood mechanism contributed to N_2O formation. We think that the Eley-Rideal mechanism is suitable for explaining the reactions in this paper [52, 53]. Firstly, NH_3 is absorbed onto the surface of GO, which can then react with Mn_2O_3 Lewis acid sites. Thus NH_2 is formed. This reaction pathway has been widely accepted in the selective catalytic reduction of NOx. Then NH_2 can be readily oxidized by HNO_3/NO_3^- to form N_2O.

Hence, we think that the probable reaction is as shown in (Reaction 2). It is also the reason why the AN with Mn_2O_3/GO sample was exothermic.

$$HNO_3/NO_3^- + NH_2 \rightarrow N_2O + H_2O \quad (2)$$

From Figure 14, we find that N_2O is formed and destroyed, most notably at about 200 °C. However, why is this species destroyed?

There was a need to understand the characteristics of nano-composites, especially GO. As is well known, GO sheets are covered with epoxy and hydroxyl groups, while carboxyl and carbonyl groups are located at the edges. These functional groups, acting as anchor sites, enable species to become attached on the surfaces and edges of GO sheets in nano-composites by hydrog-bonding. Hence, it was necessary to investigate the thermal stability of GO. The results are listed in Figure 15. We found that GO exhibited an exothermic peak at about 180 °C. This can be attributed to the decomposition of the labile functional groups, according to the DSC curve [17]. Many other researchers have also found the same results [54-56]. In other words, when the temperature exceeds 200 °C, the functional groups of GO can be destroyed. The nano Mn_2O_3 that is supported on the GO sheets *via* inter-molecular hydrogen-bonding or covalent coordination bonding would become detached from the GO [57]. This means that the interaction between Mn_2O_3 and GO is very weak and is easily destroyed. Hence, when the temperature exceeds 200 °C, the functional groups of GO are destroyed stepwise and the interactions between Mn_2O_3 and GO are also weakened. On the other hand, an exothermic reaction was observed in the decomposition of pure GO. However, when 2% GO was added to AN, the amount of heat released by GO cannot compensate the huge endothermic reaction of AN. Figure 15 shows the

result of AN with GO. Hence, we can conclude that the exothermic reaction of the AN mixture was caused by Mn_2O_3/GO, not GO. For the huge endothermic reaction of AN dissociation, the exothermic reaction of GO has little effect on the AN decomposition. In other words, the interaction between GO and AN can be ignored. But it has a notable influence on Mn_2O_3 aggregation. Hence, this is a very important factor in AN thermal decomposition, which was perhaps a key reason why the exothermic reaction of the AN mixture disappeared. The important question was how the exothermic reaction occurs and why it disappears.

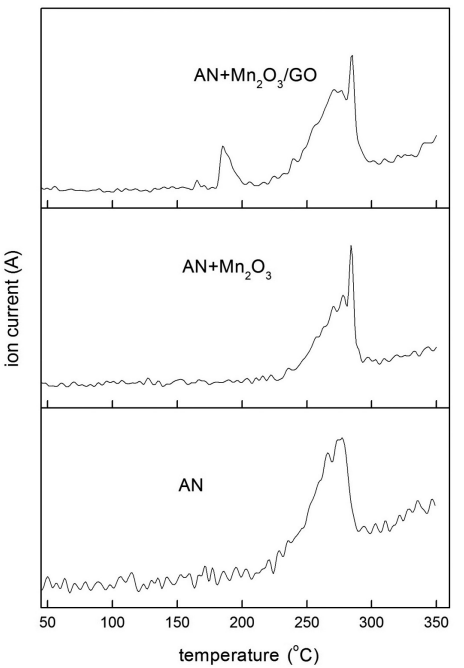

Figure 14. Ion current curve of N_2O (m/z = 44)

Based on the above analysis, we think an important factor is HNO_3 (g). As is well known, acids significantly catalyze AN decomposition [58]. The dissociation reaction of AN occurs at very low temperatures, even below the melting point of AN [36]. When GO is present, ammonia and HNO_3 (g) are adsorbed onto the GO and AN particles. When NH_3 reacted with the Mn_2O_3 to form NH_2, excess HNO_3 (g) accumulated on the surface of the GO and AN particles. Hence, the AN catalytic reaction, catalyzed by HNO_3, occurred at very low temperatures. The reaction caused a marked exothermic reaction [57]. However, with increased temperature, the HNO_3 (g) would escape from the AN particles and AN would

become liquefied, and the GO would be destroyed under the present experimental conditions. The reaction would be disappeared. Hence, HNO_3 is a very important factor for AN thermal decomposition in this study.

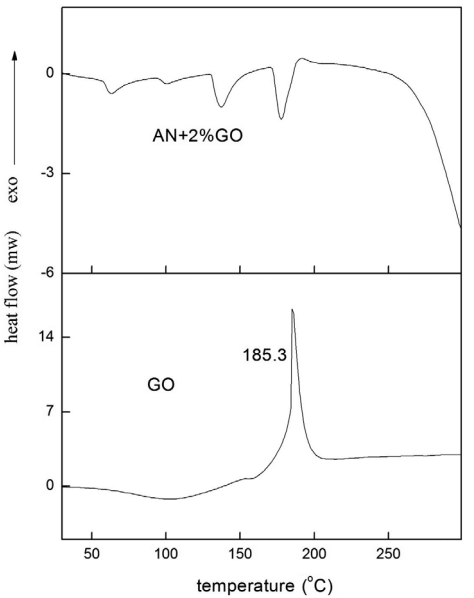

Figure 15. DSC curves of GO with and without AN

According to the above experimental results, we can summarize the mechanism of AN thermal decomposition with additives. AN starts to dissociate at very low temperature. NH_3 is adsorbed on the GO surface, and reacts with Mn_2O_3 to form NH_2. NH_2 is then oxidized by HNO_3 or NO_3^- to form N_2O. An exothermic reaction was observed in the DSC curve. However, at this temperature, the functional groups of GO are destroyed stepwise. The weak interaction between GO and Mn_2O_3 is destroyed. Hence the process of NH_2 generation is destroyed. Mn_2O_3 can still catalyze AN thermal decomposition, but the reaction rate is decreased. Moreover, HNO_3 absorbed on the surface of the AN particles, catalyzes AN thermal decomposition, and causes the exothermic reaction to occur. With HNO_3 escaping and AN liquifying, the exothermic reaction ceases. Hence, the destruction of the functional groups on GO and HNO_3 catalysis are key factors for the exothermic reaction of AN at very low temperatures. A schematic of the probable reaction mechanism of AN with Mn_2O_3/GO is shown in Figure 16.

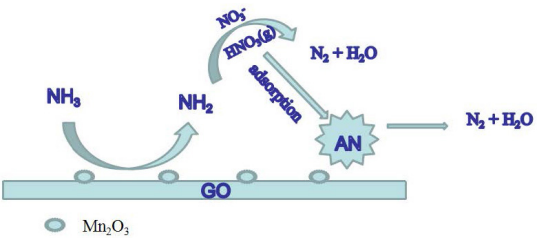

Figure 16. The probable mechanism for AN with Mn_2O_3/GO

4 Conclusions

In this paper, Mn_2O_3 and Mn_2O_3/GO nano-composites were successfully obtained by a new emulsion combustion method and they exhibited a marked catalytic effect on the thermal decomposition of AN. The nano-composites were characterized by XRD and HRTEM. The peak temperature and activation energy of AN with additives were markedly decreased, especially with Mn_2O_3/GO. An exothermic reaction phenomenon was first observed in the thermal decomposition of AN with Mn_2O_3/GO, at about 185 °C. According to the TG-MS results, this was ascribed to N_2O formation. We thought this was formed by a HNO_3/NO_3^- and NH_2 reaction at low temperature. In the RSFTIR experiments, the dissociation reaction and ionization reaction were all detected. We also found that at elevated temperatures, the functional groups of GO were destroyed stepwise, which destroyed the interaction between Mn_2O_3 and GO. We think that the fundamental reason for the exothermic reaction being eliminated was HNO_3 (g). HNO_3 catalyzes AN thermal decomposition with a marked exothermic reaction. The reason for the exothermic reaction being eliminated was also analyzed.

Acknowledgements

This paper was supported by the Inner Mogolia ShengAn Chemical Co. Ltd. and the Foundation of Jiangsu University of Advanced Scholars (15JDG159), the Natural Science Foundation of Jiangsu Colleges and Universities (16KJB150010).

References

[1] Oommen, C.; Jain, S. R. Ammonium Nitrate: a Promising Rocket Propellant Oxidizer. *J. Hazard. Mater.* **1999**, *67*(3): 253-281.

[2] Shalini, Ch.; Pragnesh, N. D. Review on Thermal Decomposition of Ammonium

Nitrate. *J. Energ. Mater.* **2013**, *31*(1): 1-26.
[3] Sinditskii, V.; Egorshev, V.; Levshenkov, A.; Serushkin, V. V. Ammonium Nitrate: Combustion Mechanism and the Role of Additives. *Propellants Explos. Pyrotech.* **2005**, *30*(4): 269-280.
[4] Xu, Z.; Fu, X.; Wang, Q. Phase Stability of Ammonium Nitrate with Organic Potassium Salts. *Cent. Eur. J. Energ. Mater.* **2016**, *13*(3): 736-754.
[5] Tomoki, N.; Makoto, K. Burning Characteristics of Ammonium Nitrate-based Composite Propellants Supplemented with Mn_2O_3. *Propellants Explos. Pyrotech.* **2013**, *38*(1): 87-94.
[6] Makoto, K.; Tomoki, N. Thermal Decomposition Behaviors and Burning Characteristics of AN/RDX-based Composite Propellants Supplemented with Mn_2O_3 and Fe_2O_3. *J. Energ. Mater.* **2015**, *33*(2): 288-304.
[7] Tomoki, N.; Makoto, K. Burning Characteristics of Ammonium Nitrate-based Composite Propellants Supplemented with Fe_2O_3. *Propellants Explos. Pyrotech.* **2013**, *38*(4): 547-554.
[8] Vargeese, A. A.; Muralidharan, K. Anatase-Brookite Mixed Phase Nano TiO_2 Catalyzed Homolytic Decomposition of Ammonium Nitrate. *J. Hazard. Mater.* **2011**, *192*(3): 1314-1320.
[9] Vargeese, A. A.; Muralidharan, K.; Krishnamurthy, V. N. Kinetics of Nano Titanium Dioxide Catalyzed Thermal Decomposition of Ammonium Nitrate and Ammonium Nitrate-based Composite Solid Propellant. *Propellants Explos. Pyrotech.* **2015**, *40*(2): 260-266.
[10] Sinditskii, V. P.; Egorshev, V. Y.; Levshenkov, A. I., Serushkin, V. V. Ammonium Nitrate: Combustion Mechanism and the Role of Additives. *Propellants Explos. Pyrotech.* **2005**, *30*(4): 269-280.
[11] Xu, Z.; Liu, D.; Hu, Y.; Ye, Z.; Wei, Y. Influence of Iron Ion on Thermal Behavior of Ammonium Nitrate and Emulsion Explosives. *Cent. Eur. J. Energ. Mater.* **2010**, *7*(1): 77-93.
[12] Kapoor, I. P. S.; Srivastava, P.; Singh, G. Nanocrystalline Transition Metal Oxides as Catalysts in the Thermal Decomposition of Ammonium Perchlorate. *Propellants Explos. Pyrotech.* **2009**, *34*(4): 351-356.
[13] Izato, Y.; Miyake, A. Combustion Characteristics of Ammonium Nitrate and Carbon Mixtures Based on a Thermal Decomposition Mechanism. *Propellants Explos. Pyrotech.* **2013**, *38*(1): 129-135.
[14] Pumera, M.; Wong, C. H. A. Graphane and Hydrogenated Graphene. *Chem. Soc. Rev.* **2013**, *42*(14): 5955-5987.
[15] Wu, Z.; Ren, W.; Wen, L.; Gao, L.; Zhao, J.; Chen, Z.; Zhou, G.; Li, F.; Cheng, H. Graphene Anchored with Co_3O_4 Nanoparticles as Anode of Lithium Ion Batteries with Enhanced Reversible Capacity and Cyclic Performance. *ACS Nano* **2010**, *4*(6): 3187-3194.
[16] Li, N.; Geng, Zh.; Cao, M.; Ren, L.; Zhao, X.; Liu, B.; Tian, Y.; Hu, Ch. Well-dispersed Ultrafine Mn_3O_4 Nanoparticles on Graphene as a Promising Catalyst for the Thermal Decomposition of Ammonium Perchlorate. *Carbon* **2013**, *54*: 124-132.

[17] Xu, Ch.; Wang, X.; Zhu, J.; Yang, X.; Lu, L. Deposition of Co_3O_4 Nanoparticles onto Exfoliated Graphite Oxide Sheets. *J. Mater. Chem.* **2008**, *18*(46): 5625-05629.
[18] Yuan, Y.; Wei, J.; Yu, J.; Shen, P.; Li, F.; Li, P.; Zhao, F.; Gao, H. Hydrothermal Preparation of Fe_2O_3/Graphene Nanocomposite and Its Enhanced Catalytic Activity on the Thermal Decomposition of Ammonium Perchlorate. *Appl. Surf. Sci.* **2014**, *303*: 354-359.
[19] Abhijit, D.; Javaid, A.; Pankaj, V.; Hima, P.; Arun, K. S.; Santanu, C. Graphene-Iron Oxide Nanocomposite (GINC): Anefficient Catalyst for Ammonium Perchlorate (AP) Decomposition and Burn Rate Enhancer for AP Based Composite Propellant. *RSC Adv.* **2015**, *5*(3): 1950-1960.
[20] Lan, Y.; Jin, M.; Luo, Y. Preparation and Characterization of Graphene Aerogel/Fe_2O_3/Ammonium Perchlorate Nano-structured Energetic Composite. *J. Sol-Gel. Sci. Tech.* **2015**, *74*(1): 161-167.
[21] Li, N.; Cao, M.; Wu, Q.; Hu, C. A facile One-step Method to Produce Ni/Graphene Nanocomposites and Their Application to the Thermal Decomposition of Ammonium Perchlorate. *Cryst. Eng. Comm.* **2012**, *14*(2): 428-434.
[22] Hu, H.; Cai, S.; Li, H.; Huang, L.; Shi, l.; Zhang, D. Mechanistic Aspects of deNOx Processing over TiO_2 Supported Co-Mn Oxide Catalysts: Structure-Activity Relationships and In Situ DRIFTs Analysis. *ACS Catal.* **2015**, *5*(10): 6069-6077.
[23] Kim, Y.; Kwon, H.; Heo, I.; Nam, I.; Cho, B. K.; Choung, J.; Cha, M.; Yeo, G. Mn-Fe/ZSM5 as a Low-temperature SCR Catalyst to Remove NOx from Diesel Engine Exhaust. *Appl Cata B: Envir.* **2012**, *126*: 9-21.
[24] Schill, L.; Putluru, S. S. R.; Fehrmann, R.; Jensen, A. D. Low-temperature NH_3-SCR of NO on Mesoporous Mn0.6Fe0.4/TiO2 Prepared by a Hydrothermal Method. *Catal Let.* **2014**, *144*(3): 395-402.
[25] Hummers, W.; Offeman, R. Preparation of Graphitic Oxide. *J. Am. Chem. Soc.* **1958**, *80*(6): 1339-1339.
[26] Ozawa, T. A New Method of Analyzing Thermogravimetric Data. *Bull. Chem. Soc. Jpn.* **1965**, *38*: 1881-1886.
[27] Xu, Z.; Pan, Z.; Zhang, P. Influence of Phosphatide on Emulsion Explosives Thermal Stability. *China Saf. Sci. J.* **2015**, *25*(5): 49-55.
[28] Wang, S.; Xu, Z.; Wang, Q. Thermal Decomposition Mechanism of Emulsion Explosives with Phosphatide. *J. Therm. Anal. Calorim.* **2016**, *124*(2): 1053-1062.
[29] Xu, Z.; Wang, Q.; Fu, X. Thermal Stability and Mechanism of Decomposition of Emulsion Explosives in the Presence of Pyrite. *J. Hazard. Mater.* **2015**, *300*: 702-710.
[30] Xu, Z.; Xu, G.; Fu, X.; Wang, Q. The Mechanism of Nano-CuO and $CuFe_2O_4$ Catalyzed Thermal Decomposition of Ammonium Nitrate. *Nanomater. Nanotechno.* **2016**, *6*: 1-10.
[31] Koga, N.; Tanaka, H. Effect of Sample Mass on the Kinetics of Thermal Decomposition of a Solid. Part 3. Non-isothermal Mass Loss Process of Molten NH_4NO_3. *Thermochim. Acta* **1994**, *240*: 141-151.
[32] Dilip, G. P.; Sampat, R. J.; Thomas, B. B. Thermal Decomposition of Energetic

Materials 56, on the Fast Thermolysis Mechanism of Ammonium Nitrate and Its Mixtures with Mangnesium and Carbon. *Propellants Explos. Pyrotech.* **1992**, *17*(3): 99-105.

[33] Brill, T. B.; Brush, P. J.; Patil, D. G. Thermal Decomposition of Energetic Materials 58. Chemistry of Ammonium Nitrate and Ammonium Dinitramide Near the Burning Surface Temperature. *Combust. Flame* **1993**, *92*(1): 178-186.

[34] Chen, H.; Wei, Z.; Kollar, M.; Gao, F.; Wang, Y.; Szanyi, J.; Peden, C. H., A Comparative Study of N_2O Formation During the Selective Catalytic Reduction of NOx with NH_3 on Zeolite Supported Cu Catalysts. *J. Catal.* **2015**, *329*: 490-498.

[35] Andersen, W.; Bills, K.; Mishuck, E.; Moe, G.; Schultz, R. D. A Model Describing Combustion of Solid Composite Propellants Containing Ammonium Nitrate. *Combust. Flame* **1959**, *3*: 301-317.

[36] Östmark, H.; Wallin, S.; Ang, H. G. Vapor Pressure of Explosives: a Critical Review. *Propellants Explos. Pyrotech.* **2012**, *37*(1): 12-23.

[37] Wu, H.; Chan, M.; Chan, Ch. FTIR Characterization of Polymorphic Transformation of Ammonium Nitrate. *Aerosol Sci. Tech.* **2007**, *41*(6): 581-588.

[38] Theoret, A.; Sandorfy, C. Infrared Spectra and Crystalline Phase Transitions of Ammonium Nitrate. *Can. J. Chem.* **1964**, *42*(1): 57-62.

[39] Izato, Y.; Miyake, A. Thermal Decomposition of Molten Ammonium Nitrate (AN). *J. Therm. Anal. Calorim.* **2015**, *122*(2): 595-600.

[40] Xu, Z.; Wang, Q.; Zhu, X.; Fu, X. Thermal Stability of Ammonium Nitrate in High-temperature Coal Seam. *J. Therm. Anal. Calorim.* **2017**, online.

[41] da Cunha, M. C. P. M.; Weber, M. I.; Nart, F. C. On the Adsorption and Reduction of NO_3^- Ions at Au and Pt Electrodes Studied by *in situ* FTIR Spectroscopy. *J. Electroanal. Chem.* **1996**, *414*(2): 163-170.

[42] Oxley, J. C.; Smith, J. L.; Rogers, E.; Yu, M. Ammonium Nitrate: Thermal Stability and Explosivity Modifiers. *Thermochim. Acta* **2002**, *384*(1): 23-45.

[43] Oxley, J. C.; Smith, J. L.; Wang, W. Compatibility of Ammonium Nitrate with Monomolecular Explosives. 2. Nitroarenes. *J. Phys. Chem.* **1994**, *98*(14): 3901-3907.

[44] Kijlstra, W. S.; Brands, D. S.; Poels, E. K.; Bliek, A. Mechanism of the Selective Catalytic Reduction of NO by NH_3 over $MnOx/Al_2O_3$. *J. Catal.* **1997**, *171*(1): 208-218.

[45] Kijlstra, W. S.; Brands, D. S.; Poels, E. K.; Bliek, A. Mechanism of the Selective Catalytic Reduction of NO by NH_3 over $MnOx/Al_2O_3$. *J. Catal.* **1997**, *171*(1): 219-230.

[46] Zhan, S.; Zhu, D.; Qiu, M.; Yu, H.; Li, Y. Highly Efficient Removal of NO with Ordered Mesoporous Manganese Oxide at Low Temperature. *RSC Adv.* **2015**, *5*(37): 29353-29361.

[47] Yang, Sh.; Qi, F.; Xiong, Sh.; Dang, H.; Liao, Y.; Wong, P.; Li, J. MnOx Supported on Fe-Ti Spinel: A Novel Mn Based Low Temperature SCR Catalyst with a High N_2 Selectivity. *Appl. Catal. B: Environ.* **2016**, *181*: 570-580.

[48] Yeom, Y. H.; Henao, J.; Li, M. J.; Sachtler, W. M.; Weitz, E. The Role of NO in the

Mechanism of NOx Reduction with Ammonia over a BaNa-Y Catalyst. *J. Catal.* **2005**, *231*(1): 181-193.

[49] Suarez, S.; Martín, J. A.; Yates, M.; Avila, P.; Blanco, J. N_2O Formation in the Selective Catalytic Reduction of NOx with NH_3 at Low Temperature on CuO-supported Monolithic Catalysts. *J. Catal.* **2005**, *229*(1): 227-236.

[50] Mihai, O.; Widyastuti, C. R.; Andonova, S.; Kamasamudram, K.; Li, J.; Joshi, S. Y. The Effect of Cu-loading on Different Reactions Involved in NH_3-SCR over Cu-BEA Catalysts. *J. Catal.* **2014**, *311*: 170-181.

[51] Tang, X.; Li, J.; Sun, L.; Hao, J. Origination of N_2O from NO Reduction by NH_3 over β-MnO_2 and α-Mn_2O_3. *Appl. Catal. B: Environ.* **2010**, *99*: 156-162.

[52] Qi, G.; Yang, R. T.; Chang, R. MnOx-CeO_2 Mixed Oxides Prepared by Co-precipitation for Selective Catalytic Reduction of NO with NH_3 at Low Temperatures. *Appl. Catal. B: Environ.* **2004**, *51*(2): 93-106.

[53] Kijlstra, W. S.; Brands, D. S.; Poels, E. K.; Bliek, A. Kinetics of the Selective Catalytic Reduction of NO with NH_3 over MnOx/Al_2O_3 Catalysts at Low Temperature. *Catal. Today* **1999**, *50*(1): 133-140.

[54] Yang, X.; Lu, Ch.; Qin, J.; Zhang, R.; Tang, H.; Song, H. A Facile One-step Hydrothermal Method to Produce Graphene-MoO_3 Nanorod Bundle Composites. *Mater. Lett.* **2011**, *65*(15): 2341-2344.

[55] Yao, Y.; Xu, Ch.; Miao, Sh.; Sun, H.; Wang, S. One-pot Hydrothermal Synthesis of $Co(OH)_2$ Nanoflakes on Graphene Sheets and Their Fast Catalytic Oxidation of Phenol in Liquid Phase. *J. Colloid Interf. Sci.* **2013**, *402*: 230-236.

[56] Shen, X.; Jiang, Ji. Zh.; Wu, J.; Zhou, H.; Zhu, G. Stable Aqueous Dispersions of Graphene Prepared with Hexamethylenetetramine as a Reductant. *J. Colloid. Interf. Sci.* **2011**, *354*(2): 493-497.

[57] Portehault, D.; Cassaignon, S.; Baudrin, E.; Jolivet, J. P. Morphology Control of Cryptomelane Type MnO_2 Nano Wires by Soft Chemistry. Growth Mechanisms in Aqueous Medium. *Chem. Mater.* **2007**, *19*(22): 5410-5417.

[58] Sun, J.; Sun, Zh.; Wang, Q.; Ding, H.; Wang, T.; Jiang, C. Catalytic Effects of Inorganic Acids on the Decomposition of Ammonium Nitrate. *J. Hazard. Mater.* **2005**, *127*(1): 204-210.